



Time-Domain Channel Estimation for the LTE-V System Over High-Speed Mobile Channels

Qu Huiyang, Liu Guanghui, Wang Yanyan, Wen Shan and
Chen Qiang

EasyChair preprints are intended for rapid dissemination of research results and are integrated with the rest of EasyChair.

May 30, 2018

Time-Domain Channel Estimation for the LTE-V System Over High-Speed Mobile Channels

Huiyang Qu, Guanghui Liu, Yanyan Wang, Shan Wen, Qiang Chen

University of Electronic Science and Technology of China, Chengdu 611731, P.R. China

Email: guanghuiqu@uestc.edu.cn, {hyqu, yywang, shanwen, qiangchen}@std.uestc.edu.cn

Abstract—Developed from the LTE uplink, the LTE-V2X standard, widely used as LTE-V, increases the overhead of pilot symbols in order to acquire channel information robustly. In this paper, we propose to estimate time-varying pieces of channel rays for pilot symbols based on the basis expansion model (BEM), and subsequently to reconstruct time-domain channel response for data symbols by utilizing Slepian sequences based piece-wise interpolation (SS-PWI). To demonstrate the precision of channel estimation (CE), the Cramer Rao lower bound (CRLB) is derived. The simulations are implemented on the LTE-V platform, on which we consider the extended vehicular A model (EVA) channel with 2800 Hz maximum Doppler shift. The proposed time-domain CE schemes are well capable of tracking the channel state information (CSI), and the mean squared error (MSE) of CE nearly reaches the theoretically derived CRLB.

Index Terms—Orthogonal frequency division multiple access (OFDMA), single carrier frequency division multiple access (SC-FDMA), long term evolution-vehicular to everything (LTE-V2X), CE, Slepian sequences

I. INTRODUCTION

Due to its advantage of low peak to average power ratio, SC-FDMA technique has been adopted as the LTE uplink transmission scheme for improving the power efficiency of mobile terminals [1]. With more pilot overhead aiming for tracking time variations of extremely high-speed mobile channel, the LTE-V standard was specified on the basis of LTE uplink framing configuration [2]. Traditionally, at the receiver side, precise CE is a necessary prerequisite for coherent demodulation, relying on inserted pilots.

When SC-FDMA is adopted by the LTE-V [3], we have to face the challenges from the CE design, especially in the vehicle to vehicle communication scenarios [4], [5]. In this case, the maximal relative velocity for the considered trials is 500 km/h, thus the maximum Doppler shift reaches 2800 Hz, given the carrier frequency of 5.9 GHz [6]. Even though much more pilot overhead is considered in the LTE-V, the frequency-domain CE schemes [7]–[9], may not capable of tracking the channel with 2800 Hz Doppler spreading.

In this paper, we address the CE challenges of the SC-FDMA with application to the LTE-V system. For the pilot symbols, each ray (i.e., path) is characterized by the basis expansion model (BEM) [10]. In the BEM, the band-limited Slepian sequences [11], are employed to express the time-varying fading channel in a low-dimensional space. Based on the estimated pieces of channel impulse response (CIR), the Slepian sequences based piece-wise interpolation (SS-PWI) is utilized for recovering the CIR of data symbols. The CRLB

of the CIR estimation is derived for the proposed channel estimator as benchmarks. The proposed time-domain CE architecture is well capable of tracking CSI while preserving a relatively low computational complexity.

The rest of this paper is organized as follows. We describe the transmission model of SC-FDMA based LTE-V system in Sec. II. In Sec. III, the proposed CE schemes are presented, which is followed by the CRLB derivation of CE in Sec. III-C. In Sec. IV, the proposed algorithms are investigated in the LTE-V receiver design and simulation results verify the proposed CE schemes. Finally, some concluding remarks are given in Sec. V.

II. SYSTEM MODEL

A discrete-time baseband SC-FDMA system with N subcarriers is considered, and ideal synchronization is assumed at the receiver side for simplicity. Without loss of generality, a single-user SC-FDMA model is considered in this paper, but the designed algorithms are applicable to the multi-user configuration. In the transmitter side (shown in Fig. 1), complex data sequence $d(k)$ is modulated by inverse fast fourier transform (IFFT) after channel encoding, constellation mapping, discrete fourier transform (DFT) and subcarrier mapping. The modulation transforms the frequency-domain data into the time-domain samples by

$$y(n) = \frac{1}{\sqrt{N}} \sum_{k=0}^{N-1} d(k) e^{j2\pi nk/N}, n \in [-N_g, N), \quad (1)$$

where $j^2 = -1$, and N_g denotes the length of the inserted the cyclic prefix (CP). The gain of the l th channel ray at the n th sampling instant is assumed: $h(n, l), l = 0, 1, \dots, L-1$, where the maximal time-delay spread $L \leq N_g$. At the receiver side, after removing CP, the received discrete-time signal is expressed as

$$r(n) = \sum_{l=0}^{L-1} h(n, l) y(n-l) + v(n), n \in [0, N), \quad (2)$$

where $v(n)$ is the zero-mean complex additive Gaussian noise with variance σ^2 .

Defining $\mathbf{r} = [r(0), r(1), \dots, r(N-1)]^T \in C^N$ and $\mathbf{y}_l = [y(-l), y(-l+1), \dots, y(N-l-1)]^T \in C^N$, the received signal is written in vector form as

$$\mathbf{r} = \sum_{l=0}^{L-1} \text{diag}(\mathbf{y}_l) \mathbf{h}_l + \mathbf{v}, \quad (3)$$

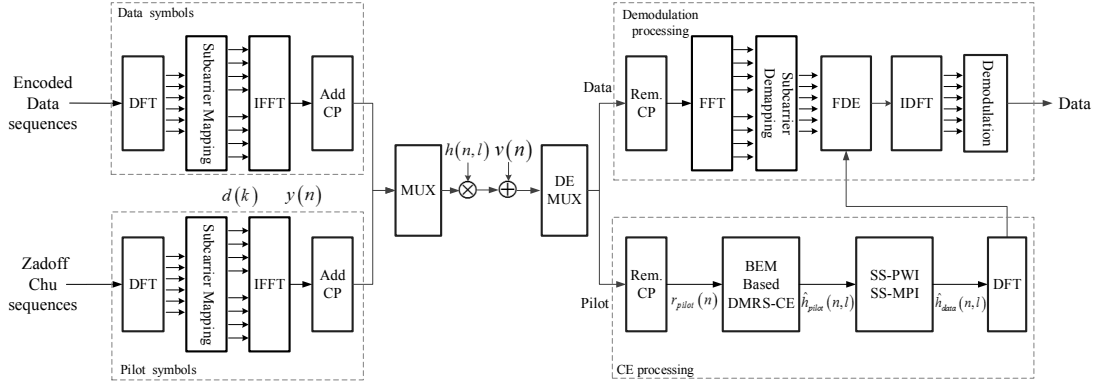


Fig. 1. Baseband model of the SC-FDMA Based LTE-V system.

where $\mathbf{v} = [v(0), v(1), \dots, v(N-1)]^T \in C^N$ and $\mathbf{h}_l = [h(0, l), h(1, l), \dots, h(N-1, l)]^T$ represents L -path WS-SUS Rayleigh fading coefficients. As the CP is employed at the transmitter, $y(-l) = y(N-l)$ for $l = 0, 1, \dots, L-1$. Assuming the Jake's model, the covariance matrix of the l th channel path is $\mathbf{R}_h(l)$, of which the elements are

$$\{R_h(l)\}_{m,n} = \sigma_l^2 r(|m-n|), \quad m, n \in [0, N], \quad (4)$$

where $r(\kappa) = J_0(2\pi f_d \kappa T_s)$. The mentioned variables $J_0(\cdot)$, σ_l^2 , f_d and T_s represent the zeroth-order Bessel function of the first kind, the normalized power of the l th channel path, the maximum Doppler spreading and the sampling period, respectively. Let $\mathbf{Y}_l = \text{diag}(\mathbf{y}_l)$, $\mathbf{Y} = [\mathbf{Y}_0, \mathbf{Y}_1, \dots, \mathbf{Y}_{L-1}]$ and $\mathbf{h} = [\mathbf{h}_0^T, \mathbf{h}_1^T, \dots, \mathbf{h}_{L-1}^T] \in C^{NL}$, (3) can be rewritten as the matrix form

$$\mathbf{r} = \mathbf{Y}\mathbf{h} + \mathbf{v}. \quad (5)$$

III. THE PROPOSED TIME-DOMAIN CHANNEL ESTIMATION SCHEMES

The LTE-V subframe structure, shown in Fig. 2, is evolved from the long term evolution-device to device (LTE-D2D), while extra two DMRS symbols are added in one subframe. The first and last symbols are used for the automatic gain control (AGC) and guard period (GP), respectively. The remained symbols are used to convey information data. From Fig. 2, the all-pilot pattern in the DMRS symbols inspires us to estimate each channel ray, of which the response is characterized by the BEM. We further use this estimated CIR to interpolate the CIR of data symbols. In this paper, CE for the AGC and GP symbols are not considered in our algorithms.

A. The Channel Estimation for Pilot Symbols

In the all-pilot DMRS symbols, the l th path of channel response within $[0, N-1]$, is represented as the weighted sum of the orthogonal basis functions $\{\varphi_d\}$ in a suitable dimension $D(\ll N)$:

$$\mathbf{h}_l = \sum_{d=0}^{D-1} c_l(d) \varphi_d = \mathbf{\Psi} \mathbf{c}_l. \quad (6)$$

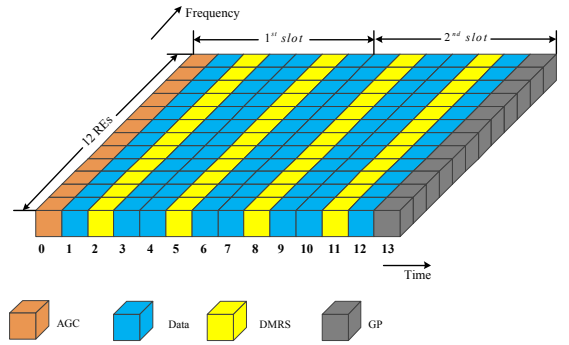


Fig. 2. Subframe structure of the LTE-V system.

In (6), $\mathbf{c}_l = [c_l(0), c_l(1), \dots, c_l(D-1)]^T \in C^D$ denotes the l th coefficient vector and $\mathbf{\Psi} \in C^{N \times D}$ is the basis-expansion matrix consisting of $\mathbf{\Psi} = [\varphi_0, \varphi_1, \dots, \varphi_{D-1}]$ and $\varphi_d = [\varphi_d(0), \varphi_d(1), \dots, \varphi_d(N-1)]^T$. The dimension D is limited by $\bar{D} \leq D \leq N$, where $\bar{D} = \lceil 2f_d T + 1 \rceil$, T is the symbol period and $f_d T$ is the maximum one-side Doppler bandwidth. Further, the channel with all taps is expressed as

$$\mathbf{h} = \mathbf{\Phi} \mathbf{c}, \quad (7)$$

where $\mathbf{c} = [\mathbf{c}_0^T, \mathbf{c}_1^T, \dots, \mathbf{c}_{L-1}^T]^T \in C^{DL}$, $\mathbf{\Phi} = \mathbf{I}_L \otimes \mathbf{\Psi} \in C^{NL \times DL}$, \otimes denotes kronecker product and \mathbf{I}_L is an $L \times L$ identity matrix. Substituting (7) into (5), the received signal is rewritten as

$$\mathbf{r} = \mathbf{Y} \mathbf{\Phi} \mathbf{c} + \mathbf{v} = \mathbf{A} \mathbf{c} + \mathbf{v}. \quad (8)$$

The desired BEM coefficient vector \mathbf{c} is subject to Gaussian distribution, i.e., $\mathbf{c} \sim N(\mathbf{0}, \mathbf{\Theta}_c)$. The covariance matrix $\mathbf{\Theta}_c = \text{blkdiag}\{\mathbf{\Sigma}_c(0), \dots, \mathbf{\Sigma}_c(L-1)\} \in C^{LD \times LD}$, where $\mathbf{\Sigma}_c(l) = \mathbf{\Phi}^T \mathbf{R}_h(l) \mathbf{\Phi} \in C^{D \times D}$ and blkdiag means the block diagonal operator [12]. For improving the accuracy of coefficients estimation, \mathbf{c} is obtained by the MMSE algorithm

$$\hat{\mathbf{c}}_{mmse} = \left(\mathbf{A}^H \mathbf{A} + \sigma^2(\mathbf{\Theta}_c)^{-1} \right)^{-1} \mathbf{A}^H \mathbf{r}, \quad (9)$$

where $(\cdot)^H$ denotes the conjugate transpose. Based on the estimated expansion coefficient vector $\hat{\mathbf{c}}$, the discrete-time

channel response could be reconstructed by (7).

In 1978, Slepian indicated that the discrete prolate spheroidal sequences, later called as Slepian sequences, demonstrated that the discrete prolate spheroidal sequences are bandlimited and simultaneously energy-concentrated in a finite time interval [11]. Specifically, the Slepian sequences are the eigenvectors of matrix $\mathbf{\Gamma} \in C^{M \times M}$

$$\mathbf{\Gamma} \varphi_i = \lambda_i \varphi_i, \quad (10)$$

where the entries of $\mathbf{\Gamma}$ are $\{\Gamma\}_{a,b} = 2 \text{sinc}\{2\pi(a-b)f_d T_s\}$ and $a, b \in \{0, 1, \dots, M-1\}$. These Slepian sequences are doubly orthogonal on the finite set $\{0, 1, \dots, M-1\}$ and the infinite set $\{-\infty, \dots, +\infty\}$ [13], definitely indicated as

$$\sum_{m=0}^{M-1} \varphi_i[m] \varphi_j[m] = \lambda_i \sum_{m=-\infty}^{+\infty} \varphi_i[m] \varphi_j[m] = \delta_{ij}, \quad (11)$$

where $i, j \in \{0, 1, \dots, M-1\}$. The eigenvalue λ_i represents the energy concentration of the i th Slepian sequence. In the BEM, we select the first D Slepian sequences as the basis functions, and simultaneously adjust the length to N . The basis functions based on the Slepian sequences are bandlimited to $[-f_d T, f_d T]$ and time-concentrated during the symbol duration $[0, N-1]$. Given f_d , the Slepian sequences are well capable of characterizing the channel response of pilot symbols.

B. Slepian Sequences Based Piece-Wise Interpolation

Inspired by the doubly-orthogonal and energy-concentrated properties, we extend the length of Slepian sequences, and subsequently approximate each channel ray with interpolation coefficients in the time interval $[0, n_3]$. Meanwhile, the dimension (i.e., number) of the extended Slepian sequences is transformed into Q , and similarly satisfies $\lceil 2f_d T_s (n_3 + 1) + 1 \rceil \leq Q \leq (n_3 + 1)$. The interpolation coefficients could be acquired by means of the estimated CIR of interval $[0, n_1]$ and $[n_2, n_3]$, which are obtained by the BEM.

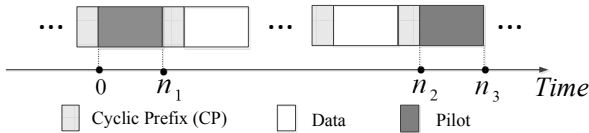


Fig. 3. The simplified LTE-V subframe structure.

For simplicity, several sets of discrete time indexing are introduced to describe the Slepian sequences based piece-wise interpolation (SS-PWI): time set of data symbols $\Delta_d = \{n_1 + 1, \dots, n_2 - 1\}$; time set of the first or left pilot symbol $\Delta_{p1} = \{0, \dots, n_1\}$; time set of the second or right pilot symbol $\Delta_{p2} = \{n_2, \dots, n_3\}$, as shown in Fig. 3. The indexes of the two pilot symbols are combined in one set as $\Delta_p = \{\Delta_{p1} \cup \Delta_{p2}\}$. Then, we have the time set of the

entire interval: $\Delta = \Delta_p \cup \Delta_d$. In the time domain, the l th channel tap is denoted as the vector $\mathbf{h}_l^\Delta \in C^{(n_3+1)}$, and

$$\mathbf{h}_l^\Delta = \left[\left(\mathbf{h}_l^{\Delta_{p1}} \right)^T, \left(\mathbf{h}_l^{\Delta_d} \right)^T, \left(\mathbf{h}_l^{\Delta_{p2}} \right)^T \right]^T. \quad (12)$$

The CIR estimates at pilot symbols $\hat{h}(n, l)$, form the vector $\mathbf{h}_l^{\Delta_{pi}}$, where $\{h_l^{\Delta_{pi}}\}_n = \hat{h}(n, l)$, $n \in \Delta_{pi}$, $i = 1, 2$. Utilizing $\mathbf{h}_l^{\Delta_{pi}}$, the piece-wise interpolation is to recover the CIR of data symbols $\mathbf{h}_l^{\Delta_d}$, where $\{h_l^{\Delta_d}\}_n = h(n, l)$, $n \in \Delta_d$.

The l th channel ray, varying during $[0, n_3]$, is expanded by the extended Slepian sequences $\{\varphi_q^e\}$ and the extended expansion parameters (i.e., interpolation coefficients) as

$$\mathbf{h}_l^\Delta \approx \sum_{q=0}^{Q-1} c_l^e(q) \varphi_q^e \approx \mathbf{\Psi}^\Delta \mathbf{c}_l^e. \quad (13)$$

In (13), $\mathbf{\Psi}^\Delta = [\varphi_0^e, \varphi_1^e, \dots, \varphi_{Q-1}^e] \in C^{(n_3+1) \times Q}$ and $\mathbf{c}_l^e = [c_l^e(0), c_l^e(1), \dots, c_l^e(Q-1)]^T \in C^{Q \times 1}$. Decomposing $\mathbf{\Psi}^\Delta$ into $\mathbf{\Psi}^{\Delta_p}$, the estimated CIR of pilot symbols satisfies

$$\mathbf{h}_l^{\Delta_p} \approx \mathbf{\Psi}^{\Delta_p} \mathbf{c}_l^e, \quad (14)$$

where $\{\mathbf{\Psi}^{\Delta_p}\}_{n,q} = \varphi_q^e(n)$, $n \in \Delta_p$, $q \in \{0, \dots, Q-1\}$ and $\mathbf{h}_l^{\Delta_p} = \{\mathbf{h}_l^{\Delta_{p1}} \cup \mathbf{h}_l^{\Delta_{p2}}\} \in C^{(n_3 - n_2 + n_1 + 2)}$. The interpolation coefficient c_l^e is obtained by using the LS method

$$\hat{\mathbf{c}}_l^e = (\mathbf{\Psi}^{\Delta_p})^\dagger \mathbf{h}_l^{\Delta_p}. \quad (15)$$

Therefore, the CIR of data symbols is recovered by

$$\hat{\mathbf{h}}_l^{\Delta_d} = \mathbf{\Psi}^{\Delta_d} \hat{\mathbf{c}}_l^e, \quad (16)$$

where $\{\mathbf{\Psi}^{\Delta_d}\}_{n,q} = \varphi_q^e(n)$, $n \in \Delta_d$, $q \in \{0, \dots, Q-1\}$.

C. Analysis of the Channel Estimation Performance

In this paper, the MMSE algorithm is utilized for the BEM coefficients estimation. Based on the analysis of CIR estimation at pilot symbols [14], in this section, we derive the CRLB of CIR estimation at data symbols based on SS-PWI.

For the l th channel tap, substituting (15) into (16), the SS-PWI can be simply expressed as

$$\mathbf{h}_l^d = \mathbf{\Psi}^d (\mathbf{\Psi}^p)^\dagger \mathbf{h}_l^p = \mathbf{B} \mathbf{h}_l^p. \quad (17)$$

For simplicity, we drop out the indexing sets Δ_d , Δ_p and use d , p to represent data and pilot indexing sets, respectively. Defining $M = n_2 - n_1 - 1$ and $2N = n_1 + n_3 - n_2 + 2$, the channel with all taps is described as

$$\mathbf{h}^d = \overline{\mathbf{B}} \overline{\mathbf{W}} \mathbf{h}^p \in C^{ML \times 1}, \quad (18)$$

where

$$\begin{aligned}
\bar{\mathbf{B}} &= \mathbf{I}_L \otimes \mathbf{B} \in C^{ML \times NL}, \\
\mathbf{h}^p &= \left[(\mathbf{h}^{p1})^T, (\mathbf{h}^{p2})^T \right]^T \in C^{2NL \times 1}, \\
\bar{\mathbf{W}} &= \left[\mathbf{W}_0^T, \dots, \mathbf{W}_l^T, \dots, \mathbf{W}_{L-1}^T \right]^T \in C^{2NL \times 2NL}, \\
\mathbf{h}^d &= \left[(\mathbf{h}_0^d)^T, (\mathbf{h}_1^d)^T, \dots, (\mathbf{h}_{L-1}^d)^T \right]^T \in C^{ML \times 1}, \\
\mathbf{h}^{pi} &= \left[(\mathbf{h}_0^{pi})^T, (\mathbf{h}_1^{pi})^T, \dots, (\mathbf{h}_{L-1}^{pi})^T \right]^T \in C^{NL \times 1}, \\
\mathbf{W}_l &= \begin{bmatrix} \mathbf{0}_{N \times lN} & \mathbf{I}_{N \times N} & \mathbf{0}_{N \times (2L-l-1)N} \\ \mathbf{0}_{N \times (L+l)N} & \mathbf{I}_{N \times N} & \mathbf{0}_{N \times (L-l-1)N} \end{bmatrix}.
\end{aligned} \tag{19}$$

Combining BEM and SS-PWI, (18) is rewritten as

$$\mathbf{h}^d = \bar{\mathbf{B}} \bar{\mathbf{W}} \begin{bmatrix} \mathbf{h}^{p1} \\ \mathbf{h}^{p2} \end{bmatrix} = \bar{\mathbf{B}} \bar{\mathbf{W}} \begin{bmatrix} \Phi & \mathbf{0} \\ \mathbf{0} & \Phi \end{bmatrix} \begin{bmatrix} \mathbf{c}_1 \\ \mathbf{c}_2 \end{bmatrix}. \tag{20}$$

Since the estimation errors exist in coefficients $\mathbf{c}_1, \mathbf{c}_2$, the interpolated CIR of data symbols is described as

$$\hat{\mathbf{h}}^d = \bar{\mathbf{B}} \bar{\mathbf{W}} \begin{bmatrix} \Phi & \mathbf{0} \\ \mathbf{0} & \Phi \end{bmatrix} \begin{bmatrix} \Xi_1 & \mathbf{0} \\ \mathbf{0} & \Xi_2 \end{bmatrix} \begin{bmatrix} \mathbf{c}_1 \\ \mathbf{c}_2 \end{bmatrix}, \tag{21}$$

where $\Xi_i = (\mathbf{A}_i^H \mathbf{A}_i + \sigma^2 (\Theta_c)^{-1})^{-1} \mathbf{A}_i^H \mathbf{A}_i$; $i = 1, 2$. The interpolation errors consist of three parts: (1) The modeling error of subspace expanded by the Slepian sequences; (2) The bias of the BEM coefficients estimation; (3) The variance of the CIR estimation introduced by BEM.

(1) The Modeling Error

In Sec. III-B, Slepian sequences are utilized for expanding a low dimensional space to characterize channels' variations. Apparently, there is an modeling error between the real and approximated channel response. The modeling error is defined as $bias_M^2$, which can be obtained from [13].

(2) Bias of the BEM coefficients estimation

The estimation bias of the BEM coefficients will also influence the Slepian interpolation. The error is defined as α , which is expressed as

$$\begin{aligned}
\alpha &= E\{\hat{\mathbf{h}}^d\} - \mathbf{h}^d \\
&= \bar{\mathbf{B}} \bar{\mathbf{W}} \begin{bmatrix} \Phi & \mathbf{0} \\ \mathbf{0} & \Phi \end{bmatrix} \begin{bmatrix} \Xi_1 - \mathbf{I} & \mathbf{0} \\ \mathbf{0} & \Xi_2 - \mathbf{I} \end{bmatrix} \begin{bmatrix} \mathbf{c}_1 \\ \mathbf{c}_2 \end{bmatrix}.
\end{aligned} \tag{22}$$

(3) The lower bound for the variance of interpolation

According to [14], the variance of the estimated BEM coefficients will affect the lower bound of CIR estimation at pilot symbols. Thereby, this variance should also be considered into the SS-PWI. By defining

$$\begin{aligned}
\mathbf{c} &= [\mathbf{c}_1^T, \mathbf{c}_2^T]^T \in C^{2DL \times 1}, \\
\mathbf{c}_A &= [\text{Re}(\mathbf{c}^T), \text{Im}(\mathbf{c}^T)]^T = [\mathbf{c}_R^T, \mathbf{c}_I^T]^T \in C^{4DL \times 1},
\end{aligned} \tag{23}$$

(21) can be rewritten as

$$\hat{\mathbf{h}}^d = \bar{\mathbf{B}} \bar{\mathbf{W}} \begin{bmatrix} \Phi & \mathbf{0} \\ \mathbf{0} & \Phi \end{bmatrix} \left\{ \begin{bmatrix} \Xi_1 & \mathbf{0} \\ \mathbf{0} & \Xi_2 \end{bmatrix} + j \begin{bmatrix} \Xi_1 & \mathbf{0} \\ \mathbf{0} & \Xi_2 \end{bmatrix} \right\} \mathbf{c}_A. \tag{24}$$

The covariance matrix of estimated coefficients \mathbf{c}_A is

$$\begin{aligned}
\mathbf{C}_L(\hat{\mathbf{c}}_A) &= E\|\hat{\mathbf{c}}_A - E(\mathbf{c}_A)\|^2 \\
&= [\nabla_{\mathbf{c}_A} E(\hat{\mathbf{c}}_A)] J^{-1}(\mathbf{c}_A) [\nabla_{\mathbf{c}_A} E(\hat{\mathbf{c}}_A)]^T,
\end{aligned} \tag{25}$$

where $J(\mathbf{c}_A)$ is the Fisher information matrix and can be obtained from [15]. The lower bound of the covariance of the interpolation processing is

$$\mathbf{C}_L(\hat{\mathbf{h}}^d) = \left\{ \bar{\mathbf{B}} \bar{\mathbf{W}} \begin{bmatrix} \Phi & \mathbf{0} \\ \mathbf{0} & \Phi \end{bmatrix} \right\} \mathbf{C}_L(\hat{\mathbf{c}}_A) \left\{ \bar{\mathbf{B}} \bar{\mathbf{W}} \begin{bmatrix} \Phi & \mathbf{0} \\ \mathbf{0} & \Phi \end{bmatrix} \right\}^H. \tag{26}$$

In summary, the lower bound of CE for data symbols is defined as CE_{CRLB} , and

$$CE_{CRLB} \geq bias_M^2 + trace\left(\alpha \alpha^H + \mathbf{C}_L(\hat{\mathbf{h}}^d)\right). \tag{27}$$

IV. SIMULATION RESULTS

In this section, simulation results are presented for assessing the performance of the proposed CE algorithms. The simulation platform is established based on the LTE-V standard. The signal bandwidth is 10 MHz, i.e., 1k system mode. The simulated channel is EVA, in which the carrier frequency is set as 5.9 GHz. Additionally, the power delay profile and parameter f_d , for configuring the designed algorithm in this paper, can be acquired by using the methods in [16], [17].

From Sec. III-C, for the ideal interpolation (i.e., the CIR at pilot symbols is ideal), the interpolation accuracy is only determined by the dimension Q . Nevertheless, in practice, the BEM based CE of pilot symbols is a prerequisite for piece-wise interpolation. The CE accuracy at pilot symbols will significantly influence the quality of interpolation. For a tradeoff between the complexity and the estimation accuracy at pilot symbols, we select $D = 5$ as the order of the BEM. Subsequently, we choose the optimal interpolation order Q through the simulations.

For obtaining the CIR in the whole subframe duration, both the intraframe and the interframe interpolators need to be implemented, which has been described in Sec. III-C. Fig. 4 gives the MSE as a function of the SNR with different interpolation orders when $f_d = 2800$ Hz, i.e., the normalized Doppler spreading is 18.6%. As shown in the figures, when considering the SNR ranging from 0 to 20 dB, the interpolating order choices for intraframe and interframe cases are $Q = 4$ and $Q = 6$, respectively. It's worth noting that, in the considered SNR range, the main estimation error is caused by the BEM. With the increasing of SNR, the MSE will converge to the modeling error of the Slepian sequence based approximation of channel response. Additionally, we choose $Q = 4$ as intra/interframe interpolation order when $f_d = 2000$ Hz.

Fig. 5 demonstrates the MSE performance of the proposed CE algorithms, when the relative mobile speeds are 500 km/h and 357 km/h, respectively. In these two cases, the SNR required by the scheme of BER+SS-PWI are about 15 dB and 10 dB at the MSE of 10^{-3} . As SNR increases, the MSE of BER+SS-PWI gradually approaches to the CRLB limit.

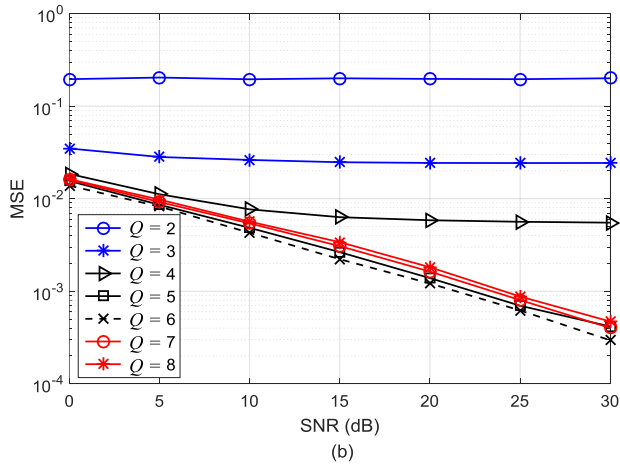
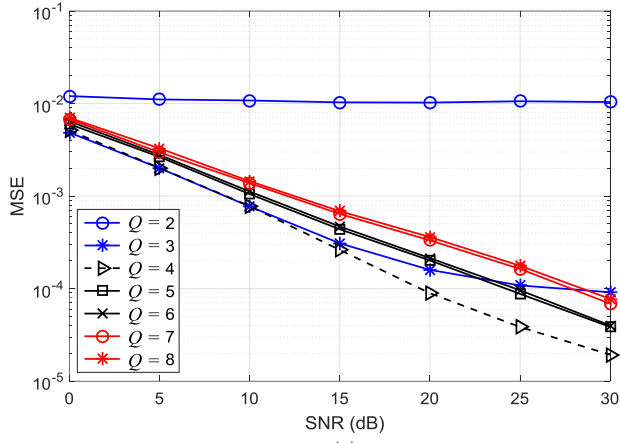


Fig. 4. The MSE vs. SNR with different interpolation orders when $f_d = 2800$ Hz. (a) Intraframe interpolation. (b) Interframe interpolation.

V. CONCLUSION

In this paper, we propose the time-domain channel estimation schemes for the LTE-V system over extremely high-speed channels. Due to the special block-type pilots structure, the basis expansion model (BEM) is utilized to obtain the CIR of pilot symbols. Subsequently, the Slepian sequences based piece-wise interpolation (SS-PWI) is employed to interpolate the CIR of data symbols. The CRLB of the CIR estimation based on the proposed estimator (BEM+SS-PWI) is also derived as benchmark for CE performance. The proposed interpolation algorithm, with the optimized orders, provides an ideal MSE performance.

REFERENCES

- [1] 3GPP, *Evolved Universal Terrestrial Radio Access (EUTRA); Physical Channels and Modulation*, Rel. 10, TS 36.211 Std., 2011.
- [2] S. Chen, J. Hu, Y. Shi, and L. Zhao, "LTE-V: A TD-LTE-based V2X solution for future vehicular network," *IEEE Internet Things J.*, vol. 3, no. 6, pp. 997–1005, Sept. 2017.
- [3] 3GPP, *Study on enhancement of 3GPP Support for 5G V2X Services*, Rel. 15, TR 22.886 (V15.1.0) Std., 2017.

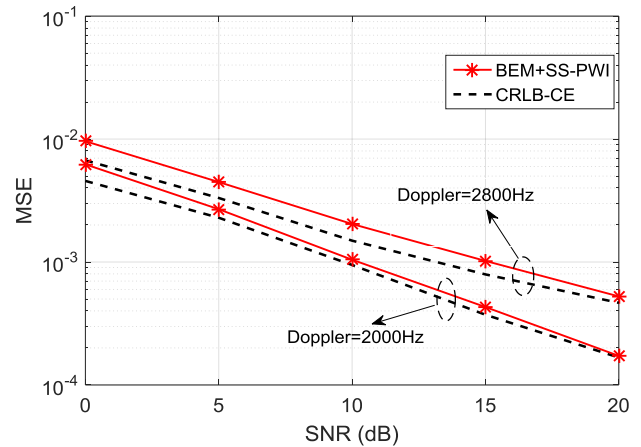


Fig. 5. MSE performance of CE when $f_d = 2800$ Hz.

- [4] W. Zhuang, "Emerging technologies, applications, and standardizations for connecting vehicles (part II)," *IEEE Veh. Tech. Mag.*, vol. 12, no. 2, pp. 23–25, May 2017.
- [5] H. Seo, K. D. Lee, S. Yasukawa, and Y. Peng, "LTE evolution for vehicle-to-everything services," *IEEE Commun. Mag.*, vol. 54, no. 6, pp. 22–28, June 2016.
- [6] S. Chen, J. Hu, Y. Shi *et al.*, "Vehicle-to-everything (V2X) services supported by LTE-based systems and 5G," *IEEE Commun. Std. Mag.*, vol. 1, no. 2, pp. 70–76, July 2017.
- [7] L. A. M. Ruiz, de Temino, C. Navarro, I. Manchon, C. Rom, and T. B. Sorensen, "Iterative channel estimation with robust wiener filtering in LTE downlink," in *Proc. IEEE VTC 2008-Fall*, Sept. 2008.
- [8] O. Edfors, M. Sandell, J. J. V. D. Beek, S. K. Wilson, and P. O. Borjesson, "OFDM channel estimation by singular value decomposition," *IEEE Trans. Commun.*, vol. 46, no. 7, pp. 931–939, July 1998.
- [9] G. Liu, L. Zeng, H. Li, L. Xu, and Z. Wang, "Adaptive interpolation for pilot-aided channel estimator in OFDM system," *IEEE Trans. Broadcast.*, vol. 60, no. 3, pp. 486–498, June 2014.
- [10] Y. Zakharov and D. Zheng, "Adaptive regularization for BEM channel estimation in multicarrier systems," in *Proc. IEEE ICASSP*, Mar. 2016, pp. 3676–3680.
- [11] D. Slepian, "Prolate spheroidal wave functions, fourier analysis, and uncertainty-V: The discrete case," *Bell Syst. Tech. J.*, vol. 57, no. 5, pp. 1371–1430, May 1978.
- [12] E. Panayirci, H. Senol, and H. V. Poor, "Joint channel estimation, equalization, and data detection for OFDM systems in the presence of very high mobility," *IEEE Trans. Signal Process.*, vol. 58, no. 8, pp. 4225–4238, July 2010.
- [13] T. Zemen and C. F. Mecklenbrauker, "Time-variant channel estimation using discrete prolate spheroidal sequences," *IEEE Trans. Signal Process.*, vol. 53, no. 9, pp. 3597–3607, Sept. 2005.
- [14] M. F. Rabbi, S. W. Hou, and C. C. Ko, "High mobility orthogonal frequency division multiple access channel estimation using basis expansion model," *IET Commun.*, vol. 4, no. 3, pp. 353–367, Jan. 2010.
- [15] E. de Carvalho and D. Slock, "Cramer-rao bounds for semi-blind, blind and training sequence based channel estimation," in *Proc. SPAWC*, Apr. 1997.
- [16] Y. J. Kim and G. H. Im, "Pilot-symbol assisted power delay profile estimation for MIMO-OFDM systems," *IEEE Commun. Lett.*, vol. 16, no. 1, pp. 68–71, Jan. 2012.
- [17] N. Linty and L. L. Presti, "Doppler frequency estimation in GNSS receivers based on double FFT," *IEEE Trans. Veh. Technol.*, vol. 65, no. 2, pp. 509–524, Feb. 2016.